

## Advancing high-speed flow simulations: SAUSM – an innovative hybrid numerical scheme for shock stability and accuracy

Adnan Mohammadi and Mohammad Hassan Djavareshkian\*

*Department of Mechanical Engineering  
Faculty of Engineering, Ferdowsi University of Mashhad  
P.O. Box 91775-1111, Iran  
\*javareshkian@um.ac.ir*

Received 1 July 2023

Revised 17 July 2023

Accepted 18 August 2023

Published 13 October 2023

This paper introduces a novel hybrid numerical method, SAUSM, designed for accurate and robust simulation of compressible flows governed by the Euler equations. While the AUSM+ scheme provides proper resolution of smooth flow features, it is susceptible to anomalies, particularly the carbuncle phenomenon near strong shock discontinuities. Conversely, the AUFS scheme offers inherent stability in capturing shocks; however, it lacks the accuracy of AUSM+ in smooth regions. The proposed SAUSM method combines AUSM+ and AUFS through an adaptive weighting function, facilitating a seamless transition between the schemes. This approach preserves the accuracy of AUSM+ in smooth regions while ensuring robust shock-capturing capabilities near discontinuities. The effectiveness of the SAUSM method is rigorously demonstrated through a comprehensive suite of progressively complex test cases. Numerical experiments demonstrate SAUSM's proficiency in resolving intense shock patterns and discontinuities without introducing anomalies. In the selected test cases, SAUSM agrees with reference solutions and effectively mitigates anomalies observed in AUSM+, including kinked Mach stems. In the challenging test case involving hypersonic blunt body flow over a cylinder, SAUSM adapts dissipation effectively by utilizing its adaptive weighting function to generate smooth pressure distributions, thereby eliminating the carbuncle instability linked to AUSM+ when applied to a high aspect ratio grid. The consistent formulation of flux splitting and the adaptive weighting in SAUSM prevent excessive dissipation away from discontinuities, thus preserving accuracy comparable to that of exact Riemann solvers. Consequently, SAUSM emerges as a promising and innovative approach to accurately and robustly simulate a wide range of compressible Euler flows. The comprehensive results obtained from the validation tests firmly establish SAUSM as a highly effective general-purpose technique for computational fluid dynamics in academic research.

*Keywords:* Carbuncle phenomenon; shock instability; kinked Mach stem; shock anomalies.

PACS number: 47.11.BC

\*Corresponding author.

## 1. Introduction

The computational algorithms used to determine the inviscid fluxes of the Euler equations for compressible flow simulations have undergone significant evolution. Central schemes were widely employed during the early 1960s and 1970s.<sup>1</sup> However, these techniques have significant drawbacks, such as a lack of accuracy in predicting the middle characteristics of flow fields and problem-dependent free parameters.<sup>2</sup> Late in the 1970s, upwind approaches were established. Upwind methods have many benefits, such as their robustness and compatibility with physical characteristics. Flux vector splitting (FVS), flux difference splitting (FDS) and AUSM (advection upwind splitting method)-type schemes are the most used upwind approaches. FVS is a natural consequence of determining fluids as a collection of particles.<sup>3</sup> Some particles will accelerate forward, while others have opposed directions at the interface. Automatically, the inviscid fluxes are decomposed into upward and downward fluxes. This decomposing method may be attained by dividing the Jacobian eigenvalue matrix. Numerous FVS methods, including Steger-Warming and Van Leer, have been given following various splitting implementations. FVS was widely used to compute the Euler equations<sup>3</sup> due to its ability to correctly and robustly determine high-gradient characteristics such as shock. Sun and Takayama<sup>4</sup> presented the AUFS approach, a specific type of FVS scheme for separating the flux vectors of Euler equations. This approach has been recently expanded<sup>5</sup> to investigate extremely high-speed flows. The AUFS system incorporates two non-real wave speeds into the flux. These two wave speeds influence the propagation direction of waves. A portion of the flow is computed numerically using the Steger-Warming method, an FVS technique. This approach is straightforward, accurate and robust for the Euler equations. Nevertheless, the scheme introduces some dissipation to shear waves in multi-dimensional flows, similar to the Steger-Warming characteristic splitting approach. This may affect the resolution of shear and boundary layers in viscous flow computations. As a result, it is an inappropriate method for solving the Navier-Stokes equations. Godunov's theory,<sup>6</sup> which postulates that the compressible flow issue between two neighboring grid cells is a local Riemann problem, is the main foundation for developing FDS schemes like Roe's FDS<sup>7</sup> and HLLE. These approaches calculate the inviscid fluxes using accurate and approximate solutions regarding Riemann's problem. Reports indicate that these approaches provide an accurate strategy for predicting discontinuities. Due to its low numerical diffusion, FDS schemes perform well in the N-S solver for resolving the boundary layer.

However, it's worth noting that while FDS methodologies are proficient in capturing discontinuities and ensuring minimal numerical diffusion for boundary layer resolution within the Navier-Stokes solver, they exhibit relatively diminished computational performance compared to their Finite Volume Scheme (FVS) counterparts. In 1991, the AUSM method was introduced, combining FVS's efficiency and FDS's accuracy.<sup>8</sup> The upwind direction of the convective values is characterized

using the method's abovementioned advection Mach number. Two pressure-splitting terms are added together to determine the pressure at the interface. The AUSM method is identified to have low numerical dissipation.<sup>8</sup> This straightforward and accurate strategy can absorb a lot of popularity and attention. The AUSM was later improved using several related techniques, including AUSM+<sup>9</sup> and AUSMPW+.<sup>10</sup> Unfortunately, the AUSM-family schemes occasionally exhibit numerical shock anomalies, including the carbuncle phenomenon. In their study, Kitamura, Roe and Ismail<sup>11</sup> conducted numerical experiments involving various flux functions to resolve hypersonic flows and observed that all of these flux functions had the potential to induce shock anomalies. The carbuncle phenomenon is a prevalent shock anomaly. In 1988, Peery and Imlay<sup>12</sup> utilized Roe's to examine the extremely high-speed flow over a blunt body and discovered specific bow shock solutions for the post of the stagnation point. Other shock wiggles include the kinked Mach stem discovered in the double Mach reflection problem and the odd-even decoupling solution identified in Quirk's test.<sup>13</sup> Low numerical diffusion methods, such as Roe's, AUSM+ and AUSMPW+, are susceptible to shock anomalies.<sup>14</sup> Even though FVS systems are immune to shock anomalies because of their high robustness, their boundary-layer resolution accuracy is insufficient. Many investigations have been conducted on shock anomalies. Pandolfi and D'Ambrosio investigated several crucial characteristics of the carbuncle phenomena.<sup>15</sup> Observations indicate that the grid aspect ratio is critical for igniting the carbuncle phenomenon. The spindly grid cells in the shock direction path contribute to anomalies. It has also been noted that this phenomenon frequently occurs whenever first-order accuracy in space is employed. Liou investigated the numerical dissipation of numerous upwind schemes and proved that the specific scheme would be free of carbuncle phenomena by eliminating the pressure term of the mass flux.<sup>16</sup> Many counterexamples to this assumption<sup>17</sup> suggest that Liou's postulate may only be practical for some systems. Xu investigated the physical cause of shock wiggles and concluded that shock instabilities did not arise on an unstructured grid.<sup>18</sup> Contrary to the findings of Ramalho *et al.*,<sup>19</sup> however. The curing of the carbuncle phenomenon is achieved through several categorized procedures. The multi-dimensional dissipation technique is followed by Roes FDS and AUSM-family schemes.<sup>20</sup> However, this approach has difficulties resolving the boundary layer.<sup>15</sup> Eigenvector modification is pursued to enhance shear wave solution and construct a robust HLL scheme<sup>21</sup>; however, eigenvector changes are scheme-specific and considerable mathematical analysis and work are required to construct these solvers. Recently, new methods were published to mitigate shock anomalies.<sup>22,23</sup> An effective approach for enhancing robustness against sudden changes in a system, known as shock anomalies, involves employing a hybrid technique introduced by Quirk.<sup>13</sup> This technique combines a dissipative scheme near a shock wave with a more accurate (less dissipative) scheme in other regions. However, the seamless integration of these two schemes may give rise to numerical challenges, such as smearing the contact interface or violating scheme positivity. The integration of robust numerical schemes from various domains, encompassing both

continuous and discontinuous phenomena, while ensuring accuracy and adaptability, has paved the way for new avenues of scholarly investigation in this field. This convergence provides researchers with a fertile ground for the development and enhancement of modern numerical approaches. A new hybrid numerical method is proposed,<sup>24</sup> which combines a full-wave Riemann solver, prone to shock instability, with the more dissipative HLL solver to eliminate numerical shock instability in simulations of the 2D Euler equations. The hybrid flux is applied only to the mass and energy equations. Numerical results demonstrate the effectiveness of the method. Nevertheless, the matrix formulation generally makes the HLL scheme more complex to implement; besides that, HLL scheme uses fixed dissipation, causing unadaptable dissipation for wide flow conditions. Moreover, blending is done only for continuity and energy equations. The justification is based on experimentation rather than theory. Besides that, the method relies on empirical constants that require tuning for different problems. A hybrid flux splitting scheme called AUSM+ FVS was proposed for compressible flows. The method combines AUSM+ and flux vector splitting to achieve accuracy in boundary layers and shock robustness.<sup>25,26</sup> This methodology finds application in diverse scenarios, such as Riemann problems and blunt body interactions, among other test cases. Notably, its performance surpasses that of the standalone AUSM+ approach. Nonetheless, it is imperative to conduct more comprehensive calibrations and analyses of the empirical coefficient ( $\beta$ ) across a range of flow regimes and Mach numbers. The authors have introduced a pivotal exponential function; however, there exists potential for additional refinement and optimization of this component through further research and experimentation. Moreover, a notable characteristic of previous FVS schemes lies in their propensity to diffuse contact discontinuities. Within the realm of previous FVS schemes, the prevalence of expansion shocks is a recurring phenomenon.<sup>4</sup> It is worth noting that the manifestation of carbuncle instability in the context of multidimensional flows raises concerns specifically associated with select FVS schemes.<sup>4</sup> AUSMV+ is blended by the Roe scheme to construct a stable method for compressible flows.<sup>27</sup> It hybridizes the Roe and modified AUSMV+ schemes using a normalized pressure/density-based weighting function to control dissipation. The hybrid Roe approach maintains Roe's accuracy while improving stability and robustness for shocks. Nevertheless, when applied to flows with strong shocks, AUSMV+ exhibits apparent shock instability issues like the carbuncle phenomenon and kinked Mach stems. This indicates that the inherent numerical dissipation of AUSMV+ is insufficient to suitably damp disturbances that cause anomalies. The minimal shock dissipation and lack of flexibility to adjust it are the primary deficiencies of AUSMV+ in shock capturing. A stable and accurate hybrid HLLC scheme for compressible flows is established by hybridizing the HLLC and modified AUSMV2+ schemes through a speed of sound-based weighting function to control dissipation.<sup>28</sup> Analysis and numerical tests show that the method damps perturbations and eliminates anomalies like carbuncles in the base HLLC scheme while maintaining accuracy. However, HLL scheme has a more expensive computational

cost than AUSM-family schemes. Besides that, AUSMV2<sup>+</sup> is dependent exclusively on the inherent low numerical dissipation stemming from its flux splitting formulations for the purpose of shock capturing. However, this constrained dissipation is frequently found to be insufficient for effectively resolving intense discontinuities, particularly shock waves, leading to anomalies.

From the abovementioned summary, hybrid methods offer a means to leverage the advantages of distinct numerical schemes, where one excels in accurately handling smooth regions while another demonstrates stability in discontinuities. A weighting function facilitates a seamless transition between these component schemes, thereby preventing anomalies like carbuncles, which may arise when employing standalone methods. By minimizing excessive dissipation away from discontinuities, hybrid approaches maintain overall accuracy. Moreover, implementing hybridization is relatively straightforward compared to developing entirely new techniques, as it permits the reuse of pre-existing, well-validated schemes as components. Consequently, hybrids provide a practical approach to enhancing stability and robustness while preserving accuracy, all at a reasonable computational cost. Several limitations have been identified in existing approximate Riemann solvers and flux vector splitting schemes for solving the Euler equations. While methods such as Roe provide accurate resolution of discontinuities, they remain susceptible to anomalies, including carbuncles and expansion shocks, necessitating additional corrections to achieve robustness. Moreover, the full characteristic decomposition in Roe's method involves matrices, adding mathematical complexity. Popular hybrid formulations like AUSMDV<sup>+</sup> and AUSMDV2<sup>+</sup> employ weighting functions skewed toward diffusivity and inconsistent splitting functions, which can reduce accuracy. Despite its computational efficiency and shock-capturing stability, the HLL scheme is overly diffusive, precluding the resolution of flow features like contact discontinuities. The motivation of this paper is to hybridize the Artificially Upstream Flux Vector Splitting (AUFVS) scheme and AUSM<sup>+</sup> scheme to remedy these deficiencies. By judiciously introducing two artificial wave speeds, AUFVS splits the physical flux vector to achieve simplicity without matrices, delivers inherent robustness against anomalies, including carbuncle instability and naturally enables resolving stationary contact discontinuities. The consistent flux splitting approach avoids weighting functions, preserving accuracy comparable to exact Riemann solvers. Moreover, the proposed SAUSM methodology demonstrates promise as an accurate and versatile technique for computational fluid dynamics applications, overcoming critical limitations of current state-of-the-art schemes.

## 2. Governing Equations

The 2D inviscid equations can be represented in a conservative form as follows:

$$\frac{\partial W}{\partial t} + \frac{\partial F^I}{\partial x} + \frac{\partial G^I}{\partial y} = 0. \quad (1)$$

$W$  is the conservative vector and  $F^I$  and  $G^I$  are the inviscid flux vectors:

$$W = \begin{bmatrix} \rho \\ \rho u \\ \rho v \\ \rho E \end{bmatrix}, \quad F^I = \begin{bmatrix} \rho u \\ \rho u u + P \\ \rho v u \\ \rho E u + P u \end{bmatrix}, \quad G^I = \begin{bmatrix} \rho v \\ \rho u v \\ \rho v v + P \\ \rho E v + P v \end{bmatrix}. \quad (2)$$

In the above equation,  $\rho$ ,  $P$ ,  $(u, v)$ ,  $E$  are density, static pressure, cartesian velocities and total energy per unit volume, respectively. The perfect gas equation is defined as follows:

$$P = (\gamma - 1) \left( E - \frac{1}{2} \rho (u^2 + v^2) \right). \quad (3)$$

### 2.1. Discretization Euler system of equations

The integral form of Euler equations around the closed boundary ( $\partial\Omega$ ) is as follows:

$$\frac{\partial}{\partial t} \iint_{\Omega} \vec{W} d\Omega + \int_{\partial\Omega} \vec{H}(\vec{W}) \cdot \hat{n} \cdot d\ell = 0, \quad (4)$$

where  $\vec{H}(\vec{W}) = \vec{F}^I(\vec{W})i + \vec{G}^I(\vec{W})j$  is the inviscid flux. By using the finite-volume methodology, Eq. (4) would be as follows:

$$\frac{d}{dt} (\vec{Q}_j \Omega_j) + \sum_{k=1}^3 \vec{H}_k \cdot d\ell_k = 0, \quad (5)$$

where  $\vec{H}_k$  is inviscid flux and computed based on the AUSM+ or AUFS schemes.

### 2.2. AUSM+ scheme

The general form of computing inviscid flux by AUSM+ is determined as follows<sup>9</sup>:

$$\vec{H}_k = \left( \frac{\dot{m} + |\dot{m}|}{2} \right) \phi_L + \left( \frac{\dot{m} - |\dot{m}|}{2} \right) \phi_R + p_{1/2}. \quad (6)$$

$$\phi = \begin{bmatrix} 1 \\ u \\ v \\ h \end{bmatrix}. \quad (7)$$

Computing the pressure flux of AUSM family can be determined as follows<sup>29</sup>:

$$p_{1/2} = \bar{p} - d_p, \quad (8)$$

where  $\bar{p}$  is the average pressure of two sides of each interface. Moreover,  $d_p$  is defined as follows:

$$d_p = \frac{1}{2} (P_L^+ - P_R^-) \Delta p + \{ (1 - P_L^+ - P_R^-) \bar{p} \}. \quad (9)$$

With  $\Delta p$  as the differential pressure ( $\Delta p = P_R - P_L$ ) and

$$P_{(L/R)}^\pm = \begin{cases} \pm \frac{(M_{(L/R)} \pm 1)^2}{4} (2 \mp M_{(L/R)}) \pm \alpha M_{(L/R)} ((M_{(L/R)})^2 \mp 1)^2 & |M| < 1, \\ \frac{M_{(L/R)} \pm |M_{(L/R)}|}{2} & |M| \geq 1, \end{cases} \quad (10)$$

where

$$\alpha = \frac{3}{16}, \quad (11)$$

$$M_{(L/R)} = (V_{(L/R)})/C_{1/2}, \quad (12)$$

$$V_{(L/R)} = u_{(L/R)} \cdot \mathbf{n}_x + v_{(L/R)} \cdot \mathbf{n}_y, \quad (13)$$

$$C_{1/2} = \begin{cases} \frac{c^{*2}}{\max(|V_L|, c^*)} & \frac{V_L + V_R}{2} \geq 0, \\ \frac{c^{*2}}{\max(|V_R|, c^*)} & \frac{V_L + V_R}{2} < 0, \end{cases} \quad (14)$$

$$c^{*2} = \frac{2(\gamma - 1)\bar{H}}{(\gamma + 1)}, \quad (15)$$

$$\bar{H} = \frac{\gamma RT}{(\gamma - 1)} + \frac{u^2 + v^2}{2}. \quad (16)$$

With “+” and “-” or “L” and “R” symbols, determine the left and right of each face, respectively. To compute mass flux according to AUSM+ scheme, the following manner is required:

$$(\dot{m})_{1/2} = C_{\frac{1}{2}} M_{\frac{1}{2}} \times \begin{cases} \rho_L & M_{1/2} > 0, \\ \rho_R & M_{1/2} < 0, \end{cases} \quad (17)$$

$$M_{1/2} = M_L^+ + M_R^-,$$

$$M_{(L/R)}^\pm = \begin{cases} \pm \frac{(M \pm 1)^2}{4} \left( 1 \mp \frac{1}{16} \beta \frac{(M \mp 1)^2}{4} \right) & \beta_{\text{AUSM}} = \frac{1}{8} & |M| < 1, \\ \frac{M \pm |M|}{2} & & |M| \geq 1. \end{cases} \quad (18)$$

### 2.3. AUFS scheme

The AUFS approach can be determined as follows<sup>4</sup>:

$$\vec{H}_k = (1 - M) \left[ \frac{1}{2} (P_L + P_R) + D_{\text{AUFS}} \right] + M [W^\beta (q^\beta - s_2) W + P^\beta], \quad (19)$$

where  $W$  is the conservative vector defined through (2) and  $P$  vector is defined as follows:

$$P = \begin{pmatrix} 0 \\ pn_x \\ pn_y \\ pq \end{pmatrix},$$

where  $q$  is the normal velocity of an arbitrary interface and is defined as follows:

$$Q = un_x + vn_y,$$

With  $[n_x, n_y]$  being the normal unit vector of a cell interface. Note that  $s_1$  and  $s_2$  are two constant scalars. Moreover,  $M = s_1/(s_1 - s_2)$  and  $s_1, s_2$  are the two artificial scalars determining wave speeds. The superscript  $\beta$  classified the left and right direction of waves propagating based on  $s_1$  sign as follows:

$$\beta = \begin{cases} L & \text{for } s_1 > 0, \\ R & \text{for } s_1 \leq 0, \end{cases} \quad (20)$$

The vector  $D_{\text{AUFS}}$  is the dissipation of the AUFS scheme and is defined as follows:

$$D_{\text{AUFS}} = \frac{1}{2C_{1/2}} \begin{pmatrix} p_L - p_R \\ (Pu)_L - (Pu)_R \\ (Pv)_L - (Pv)_R \\ \frac{(C_{1/2})^2}{\gamma - 1} (p_L - p_R) + \frac{1}{2} ((pq^2)_L - (pq^2)_R) \end{pmatrix}, \quad (21)$$

where

$$q^2 = u^2 + v^2. \quad (22)$$

The expressions for computing  $s_1$  and  $s_2$  are determined by Sun and Takayama<sup>4</sup> and defined as follows:

$$s_1 = \frac{1}{2} (q_L + q_R), \quad (23)$$

$$s_2 = \begin{cases} \min(0, q_L - C_L, q^* - c^*) \\ \max(0, q_R + C_R, q^* + c^*) \end{cases}, \quad (24)$$

where:

$$q^* = \frac{1}{2} (q_L + q_R) + \frac{C_L - C_R}{\gamma - 1}, \quad (25)$$

$$c^* = \frac{1}{2} (c_L + c_R) + \frac{(q_L - q_R)(\gamma - 1)}{4}. \quad (26)$$

#### 2.4. Hybrid scheme

The SAUSM scheme is developed by hybridizing AUSM+ and AUFS schemes. The AUSM+ scheme is a low dissipation scheme with high resolution in all flow fields

except the shock region, while the AUFS is free from shock anomalies in the vicinity of the shock region. Therefore, SAUSM is designed to be an averaging scheme with a bias toward the AUFS scheme to take advantage of the shock-capturing capability of AUFS scheme as follows:

$$\vec{H}_k = \frac{1}{2} [((\vec{H}_k)_{\text{AUFS}} + (\vec{H}_k)_{\text{AUSM+}}) - F((\vec{H}_k)_{\text{AUSM+}} - (\vec{H}_k)_{\text{AUFS}})], \quad (27)$$

where  $F$  is the weighting switch function.

This paper determines the new weighting switch function by a normalized pressure-to-density ratio of an arbitrary cell interface.<sup>27</sup>

$$F = 2 \min(1, G) - 1. \quad (28)$$

$$G = \begin{cases} \left| \frac{P_r}{\rho_r} - \frac{P_l}{\rho_l} \right| & (q - c)(q + c) < 0, \\ 0 & \text{otherwise,} \end{cases} \quad (29)$$

where  $P_{r/l}$ ,  $\rho_{r/l}$  are defined as follows:

$$P_{r/l} = \frac{P_{R/L}}{P_\infty}, \quad (30)$$

$$\rho_{r/l} = \frac{\rho_{R/L}}{\rho_\infty}, \quad (31)$$

where infinity subscript denotes defined free-stream values, Eq. (29) is weighted toward the AUFS scheme in the region of shock waves; however, the weight is pushed toward the AUSM+ scheme elsewhere to obtain a highly accurate solution. In the smooth regions of the flow field without any sharp gradients and contact discontinuity areas, the original AUSM+ system is implemented.

### 3. Time-Marching Strategy

It is evident that by implementing the integration to governing equations in a control volume, the spatial and transient terms are separated, and a set of ordinary equations is established as follows:

$$\frac{d}{dt} (W_i) + R_i(W) = 0. \quad (32)$$

$R_i$  is the integrated spatial term, and  $W$  is the conservative term. To achieve the solution of the above equation, it is required to implement time integration to governing equations. The method of transient discretization of the above equation in this study is the explicit 4th-order Runge-Kutta strategy.

### 4. Numerical Experiments

This section aims to systematically validate the accuracy, robustness and versatility of the SAUSM scheme across a wide range of compressible flow regimes.

The validation begins by considering elementary 1D Riemann problems involving typical discontinuities. This serves as a basis for assessing the scheme's capability to capture shocks accurately. Subsequently, a 2D Riemann problem is introduced to evaluate its performance in resolving multi-dimensional oblique shock interactions. The evaluation continues with examining the Double Mach reflection case, which tests the stability of the scheme in handling complex shock reflections occurring in practical geometries. This scenario is known to challenge non-robust solvers due to anomalies. Finally, a stringent simulation of hypersonic flow over a cylinder is conducted, exposing the scheme to a strong bow shock to assess its resilience against instabilities, such as the carbuncle phenomenon often encountered in low-dissipation methods. It is important to note that the test suite progressively increases in complexity, advancing from canonical 1D shocks to geometrically intricate flows prone to anomalies. This comprehensive approach thoroughly scrutinizes SAUSM's performance across various challenges, including basic shock-capturing, nuanced multi-dimensional discontinuity resolution, stability in complex configurations and resilience against prevalent anomalies. These systematic evaluations confirm SAUSM's accuracy in resolving typical shock patterns, ability to capture multi-dimensional discontinuities with high fidelity, stability even in intricate flow scenarios and robustness against instabilities. This rigorous validation establishes SAUSM as a practical, accurate, stable and versatile technique for conducting diverse compressible Computational Fluid Dynamics (CFD) simulations.

#### 4.1. *One-dimensional Riemann problem*

A Sod shock tube problem<sup>30</sup> was first taken into consideration. A Riemann issue is a problem with an initial value determined by a conservation equation. Often, the field is split at the initial time by constant states. Shock and reflecting waves demonstrate crucial features in the solution; the Riemann problem is beneficial for investigating numerical procedures for computing the Euler form of governing equations. The one-dimensional Riemann matter is frequently applied to the analysis of numerical methods. At the start of the test, the region of computing has two constant states:  $(\rho, u, p)_L$  and  $(\rho, u, p)_R$ . The discontinuity has been located at the position  $x = 0.0$  and the Courant number coefficient has been assigned a value of  $CFL = 0.9$ . This one-dimensional examination is implemented in the field  $x \in [-22, 22]$ . The initial conditions are

$$\begin{aligned}(\rho, u, p)_L &= (10.14543, 0, 2 \times 10^6) \quad x \in [-22, 0]. \\(\rho, u, p)_R &= (1.216136, 0, 0.2 \times 10^6) \quad x \in [0, 22].\end{aligned}$$

First-order accuracy is adopted concerning spatial terms. Figure 1 depicts the density, pressure, temperature and velocity profiles at time 0.0196s derived by AUSM+ and AUFS. The analytical solution, shown by the black line in the picture, is included for reference. The 1D Riemann problem results reveal that the SAUSM scheme successfully preserves the essential discontinuity-capturing capabilities and

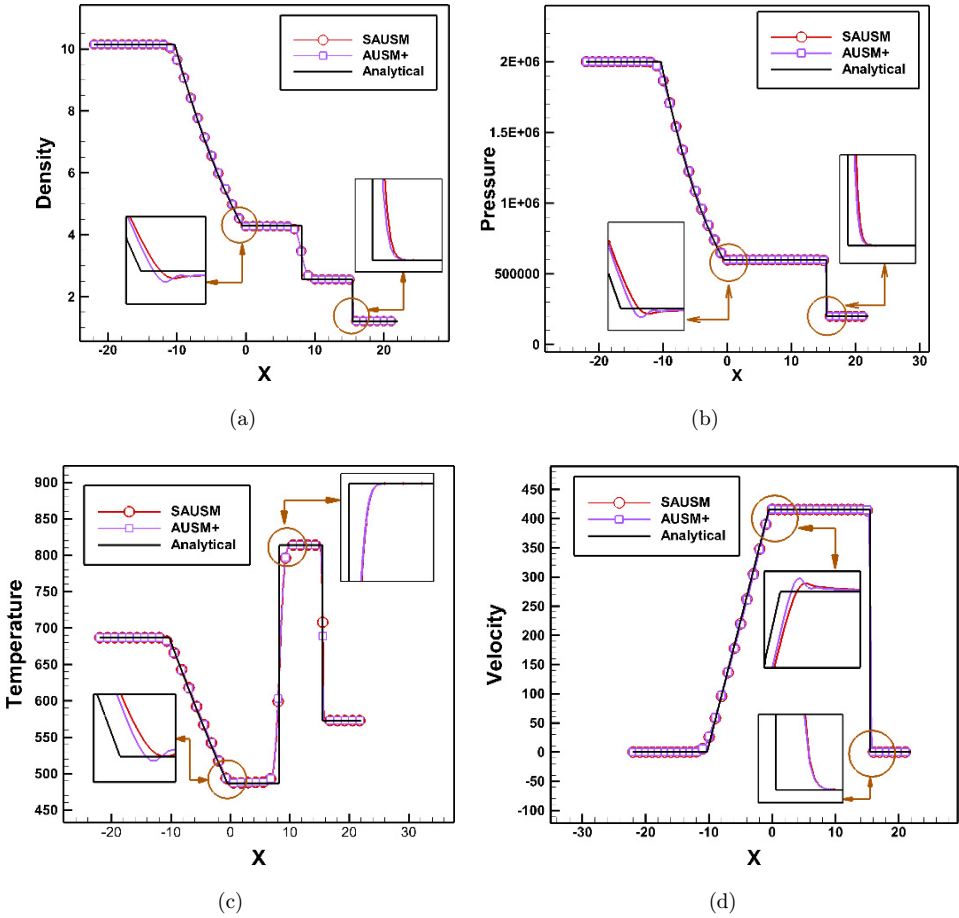


Fig. 1. Distribution of flow field characteristics pertaining to one-dimensional Riemann problem test case. (a) Density, (b) pressure, (c) temperature and (d) velocity.

underlying accuracy of the AUSM+ scheme for resolving fundamental shock and contact surface structures. This is evidenced by the near exact overlap of the SAUSM and AUSM+ density, pressure, temperature and velocity profiles across the full span of the flow field, with minor discrepancies tightly confined to the immediate shock region. The close alignment of both schemes with the analytical solution profiles verifies SAUSM's proficiency in inheriting AUSM+'s fidelity for 1D test cases through its consistent flux-splitting formulation and seamless hybridization procedure. Critically, SAUSM can decrease subtle oscillatory instabilities produced by AUSM+ in the smooth expansion fan region without significantly compromising its accuracy at discontinuities. This is achieved through the intrinsic numerical diffusion of SAUSM's hybridized methodology. The additional selective dissipation damps out the minor wiggles and overshoots exhibited by AUSM+ in the expansion fan by

taking advantage of the flexibility of SAUSM’s weighting function. This allows for minimizing the impact on accuracy at the shock and contact surface. Therefore, the 1D Riemann problem findings substantiate SAUSM’s proficiency in replicating AUSM+’s high-fidelity discontinuity resolution for basic 1D flows while augmenting stability through its hybrid formulation. The results validate SAUSM’s capabilities in capturing essential shock patterns without compromising accuracy or introducing excessive diffusion. This establishes a robust basis for applying SAUSM’s approach to inherently unstable higher-dimensional cases.

#### 4.2. Two-dimensional Riemann problem

Unsteady two-dimensional (2-D) Lax configuration3 is explored for the following test scenario. This particular setup and other configurations had been extensively examined in<sup>30,31</sup> and embraced as well-regarded benchmark test problems. This problem was highly nonlinear, involving the formation of the upward-moving jet, the downward-moving mushroom jet and secondary Kelvin-Helmholtz instabilities exhibited as small-scale vortical rollups along the slip lines and the stems of the two jets. This Complex particular benchmark test case is used to assess the effectiveness of the AUSM+ and SAUSM schemes. Lax and Liu have presented 19 combinations.<sup>32</sup> For further information on the wave structures of each configuration for other benchmark test cases, a reference was made to their archived paper. At the domain’s boundaries, the normal gradients of all flow variables were required to be zero. Considering virtual cells outside the borders was a common approach to implementing boundary conditions. The first-order virtual reflexive boundary

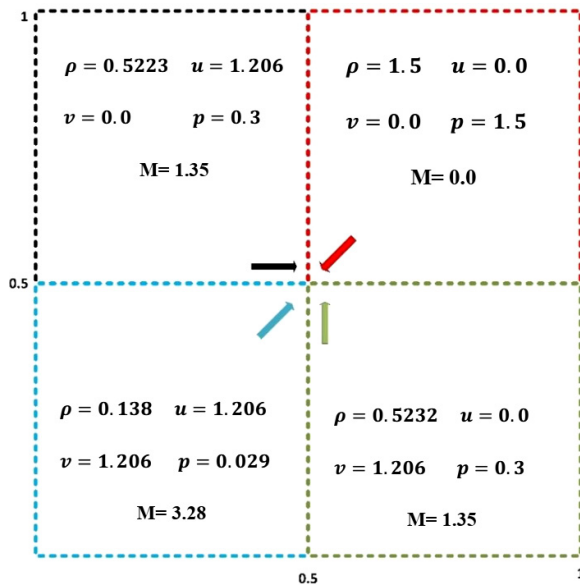


Fig. 2. Initial condition of two-dimensional Riemann problem (Lax configuration3).

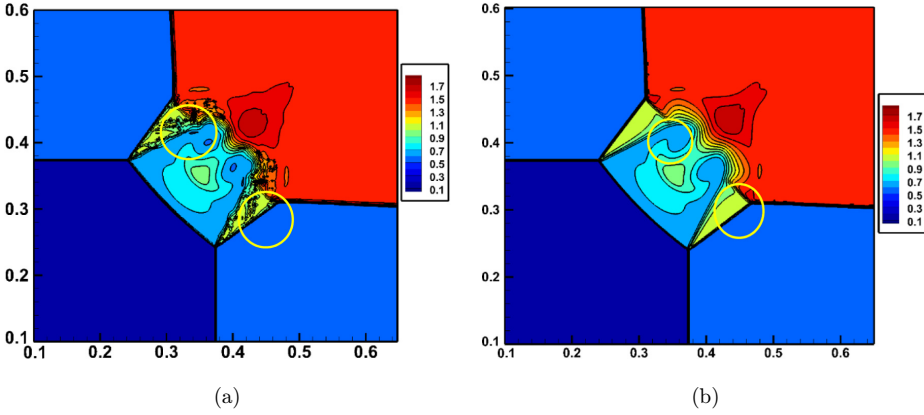


Fig. 3. Density distributions of two-dimensional Riemann problems. (a) AUSM+ scheme. (b) SAUSM scheme.

condition is used for a wall where the cells terminate. Figure 2 shows the initial condition of the Lax configuration<sup>3</sup>.

A meticulous examination of the AUSM+ solution depicted in Fig. 3(a) exposes conspicuous deficiencies characterized by localized warping and distortion of the density contour lines spanning the entire flow field, as the yellow circle annotation underscores. These subtle yet perceptible anomalies can be attributed to the inherent numerical dissipation insufficiency adjacent to shock discontinuities when employing AUSM+ in isolation, which has been extensively scrutinized in prior research endeavors.<sup>33</sup> This insufficiency in dissipation facilitates the rapid amplification of minor perturbations when shock fronts align with the grid lines, thereby inciting instabilities. In stark contradistinction, the outcomes presented in Fig. 3(b), arising from the application of SAUSM, showcase remarkably smooth and continuous density contours devoid of any warping or anomalies. The faithful depiction of the morphology of the mushroom-shaped jet is achieved without any observable distortions. Of particular note is the heightened acuity with which SAUSM resolves the Mach stem shocks; any subtle anomalies are conspicuously confined to the immediate vicinity of the Mach stems. The density distribution maintains uniformity even amidst the presence of shocks, thereby affirming the exceptional shock-capturing robustness inherent to SAUSM. This notable enhancement emanates from the hybrid formulation employed by SAUSM, which judiciously introduces supplementary stabilization through the AUFS component in proximity to abrupt discontinuities, such as shocks. The resultant supplementary dissipation effectively curtails the amplification of instability-inducing perturbations that engender anomalies within the framework of AUSM+. The complete absence of such anomalies and the meticulous portrayal of intricate flow structures within the SAUSM solution unequivocally validate its reliability in faithfully simulating intricate multi-dimensional shock hydrodynamics while circumventing the stability limitations characteristic of AUSM+.

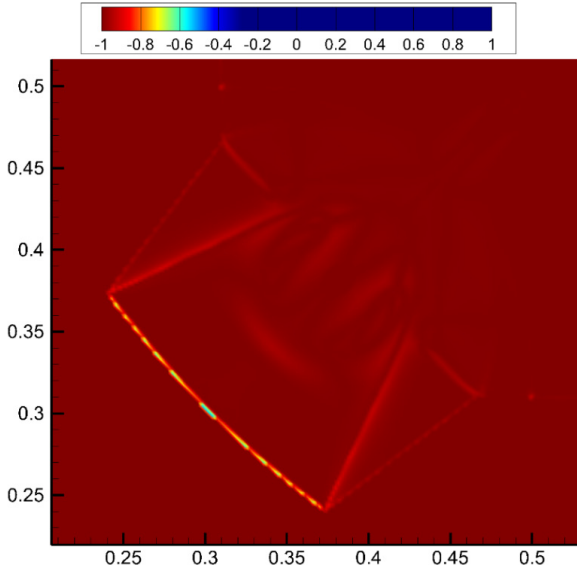


Fig. 4. The contour of the weighting function for a two-dimensional shock tube.

The weighting function  $F$  is fundamental to SAUSM’s ability to deliver shock stability and accuracy by seamlessly blending the AUSM+ and AUFS component schemes. It provides adaptive control tailored to local flow conditions. In smooth regions away from discontinuities,  $F$  trends towards  $-1$ , emphasizing the low-dissipation AUSM+ scheme. This maintains the high-fidelity resolution of flow features. Near shocks and other discontinuities,  $F$  shifts towards  $1$ , leveraging the inherent robustness of AUFS (Fig. 4). The artificial dissipation in AUFS suppresses instabilities that cause anomalies. The smooth transition between AUSM+ and AUFS enabled by  $F$  avoids sharp changes in dissipation that reduce accuracy. In areas where anomalies intensify, like near interactions of shocks,  $F$  further increases the AUFS weighting to enhance stability. The adaptive distribution of  $F$  provides customized blending based on the local balance of accuracy and stability needed. Moreover, the field of  $F$  visualized in Fig. 4 demonstrates how SAUSM achieves shock-capturing capabilities and accuracy.  $F$  provides continuous control between these attributes tailored to flow conditions. This is essential for simultaneously resolving smooth flow features without anomalies at discontinuities. The contour plot validates the effectiveness of  $F$  in enabling SAUSM’s high-fidelity and versatile performance.

### 4.3. Double mach reflection problem

Several numerical methods have been reported to yield kinked Mach stems in the double Mach reflection scenario. Woodward and Colella<sup>34</sup> were the first to study it, followed by several other academics. According to the figure, a normal shock

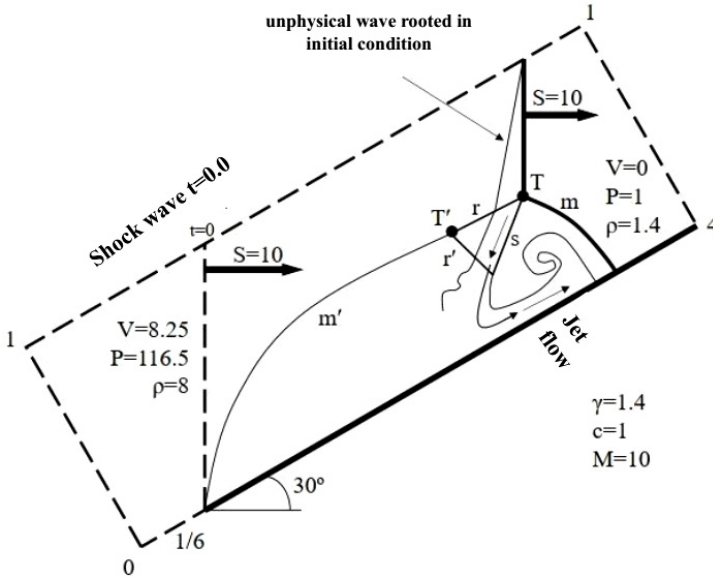


Fig. 5. Reflection of normal shock by a 30° ramp.

reflected by a 30° slope is considered unsteady. The incident shock wave remains unchanged as it reflects off the sloped wall and then moves up the wedge. When the primary shock wave follows the correct path, it leads to the formation of a reflected shock wave ( $r$ ), a Mach stem ( $m$ ) and a slip line ( $s$ ) originating at the triple point, determining the original Mach reflection. The triple point ( $T'$ ) is created at the intersection of the primary reflection ( $r$ ), the secondary reflection ( $r'$ ) and the curved stem ( $m'$ ), resulting in the formation of the second Mach reflection.

The computational domain is  $[0, 4] \times [0, 1]$ , with 400 cells along the length and width. The domain after the shock initiates with the values  $\rho = 1.4$ ,  $u = 0$ ,  $v = 0$  and  $p = 1$  before the shock. The field behind the shock is initialized with values before the shock. The computations utilize first-order numerical methods and fourth-order Runge-Kutta temporal discretization up to  $t = 0.2$  s. In real-world experiments and high-fidelity simulations, the Mach stem forms a straight oblique shock attached to the reflection surface. The kinked distortion of the Mach stem does not occur. The kink allows post-shock flow along the surface to spill out ahead of the Mach stem, causing non-physical flow patterns. Real Mach stems do not show this behavior.<sup>35</sup> Methods that produce kinked Mach stems are considered unreliable for predicting complex shock reflections. The results can be misinterpreted if anomalies are not addressed. Kinked Mach stems are regarded as a numerical artifact rather than fundamental physics. Their appearance indicates issues with the solver's robustness and accuracy. Insufficient numerical dissipation when shocks are aligned with grid lines. This allows perturbations to develop due to a lack of cross-dissipation between grid points.<sup>13</sup> Shortcomings in the mathematical expression for the internal structure

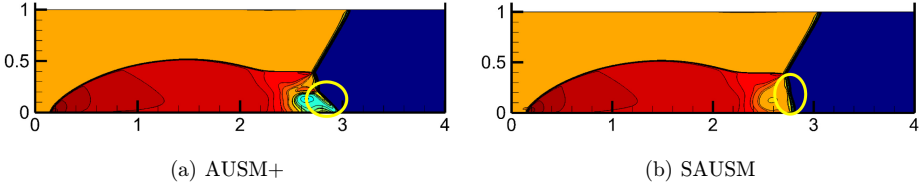


Fig. 6. The density contours for double Mach reflection problem at  $t = 0.2$  s.

of captured shock waves in numerical methods are found. This causes anomalies when the shock transitions between grid lines. Figure 6 depicts the density contours estimated by AUSM+ and SAUSM techniques, with 30 contour levels ranging from 2.0 to 20.0. Established empirical and computational evidence underscores several vital features of the envisioned shock configuration. These features include the incident shock itself, the primarily reflected shock resulting from interaction with the inclined ramp, an oblique Mach stem displaying nearly linear characteristics that connect to the point of reflection of the primary triple junction, and a subsequent emanating slip line. Notably, the density contour plot of the AUSM+ scheme reveals an identifiable anomaly (highlighted by the yellow circle) in the trajectory of the Mach stem, characterized by a distinctive kinked distortion. This aberration can be attributed to inadequate inherent shock dissipation within the AUSM+ scheme.<sup>33</sup> The insufficiency of intrinsic dissipation allows disruptive perturbations to magnify when shock fronts align with grid lines due to the absence of cross-dissipative mechanisms. Consequently, an anomalous non-physical post-shock flow outflow emerges before the kinked Mach stem. In contrast, the numerical outcomes yielded by the SAUSM scheme depict a Mach stem that remains consistently rectilinear and uninterrupted, devoid of distortions (indicated by the yellow circle). This result underscores the heightened robustness and stability intrinsic to the SAUSM scheme, qualities that stem from its well-balanced hybrid formulation. This formulation strategically introduces supplementary accurate dissipation near shock phenomena by leveraging the AUFS component. As a result, the SAUSM scheme effectively suppresses the amplification of perturbations responsible for anomalies like the kinked Mach stem observed in the AUSM+ counterpart.

Figure 7 presents a contour plot illustrating the characteristics of the weighting function  $F$ , as defined in Eq. (28) of the paper. The data depicted pertains to the Double Mach reflection test, and its computation employs the proposed SAUSM scheme. This weighting function operates adaptively, imparting a bias to the scheme towards AUSM+ or AUFS, contingent upon the prevailing local flow conditions. Within Fig. 7, the weighting function demonstrates a propensity to approach a value of 1 in proximity to instances of discontinuity, such as strong shock waves and contact surfaces. This strategic behavior shifts the emphasis of flux computation towards the employment of the AUFS scheme. Notably, the AUFS scheme boasts higher accuracy and inherent robustness in handling such regions. This particular

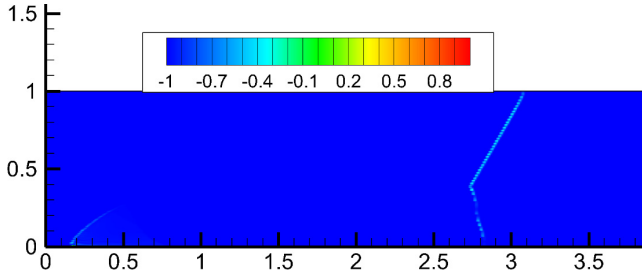


Fig. 7. The contour of the weighting function for Double Mach reflection problem.

mechanism intrinsic to AUFSS is instrumental in mitigating instabilities at points of discontinuity. Consequently, anomalies such as kinked Mach stem, observed when utilizing AUSM+ in isolation, are effectively eradicated. Contrastingly, in areas characterized by smooth flow devoid of discontinuities, the weighting function tends to trend towards a value of  $-1$ , which is visually represented by the blue regions in the plot. This emphasis towards  $-1$  underscores the application of the low dissipation AUSM+ scheme. Overall, Fig. 7 affords a comprehensive visual representation of the dynamic nature of the weighting function  $F$  within the context of the SAUSM scheme. Its adaptability based on local flow conditions optimizes the selection between AUSM+ and AUFSS, thereby enhancing the accuracy and stability of flux computations across varying regions of the flow field.

#### 4.4. Hypersonic inviscid flow over a cylinder

To illustrate the shock-stable performance of the suggested SAUSM method, hypersonic inviscid flow at Mach = 10 over a cylinder is provided. The renowned carbuncle phenomena<sup>13</sup> have been reported for several upwind schemes in hypersonic blunt body simulations. Several publications<sup>11,36</sup> have revealed that the aspect ratio of cells significantly affects the inducing carbuncle instability. To further demonstrate the usefulness of the SAUSM approach, in Fig. 8, the geometry of the cylinder depicts a grid with 39 (wall normal) and 501 (radial) grid points and a high aspect ratio of cells. Grids with high aspect ratios hinder the exchange of dissipation effects across neighboring cells, thereby permitting the unhindered propagation of disruptive waves.<sup>15</sup> The simulations use an explicit time marching technique and a first-order accuracy spatial approach. Figure 9 presents pressure contour plots extracted from hypersonic cylindrical blunt body flow simulations at Mach 10, employing both AUSM+ and SAUSM schemes. In this canonical test case, a robust bow shock forms at the stagnation region on the forward-facing surface of the cylinder. A closer examination of the AUSM+ results reveal the emergence of a well-documented numerical shock instability known as the ‘carbuncle phenomenon.’ This instability is evident as the bow shock exhibits an anomalous bifurcation and a discontinuous split near the stagnation point, as indicated by the highlighted yellow circle. Several factors

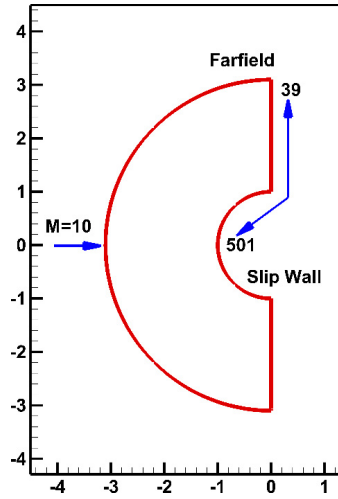


Fig. 8. Geometry of cylinder.

contribute to this carbuncle phenomenon with AUSM+: reliance solely on the left-state density for computing interface mass flux, leading to inaccuracies near strong shock gradients; inadequate inherent pressure dissipation allowing non-physical expansion shocks to form adjacent to the primary bow shock, disrupting its structure; lack of appropriate velocity-weighting in the pressure flux expression rendering AUSM+ susceptible to shock anomalies at high Mach numbers; utilization

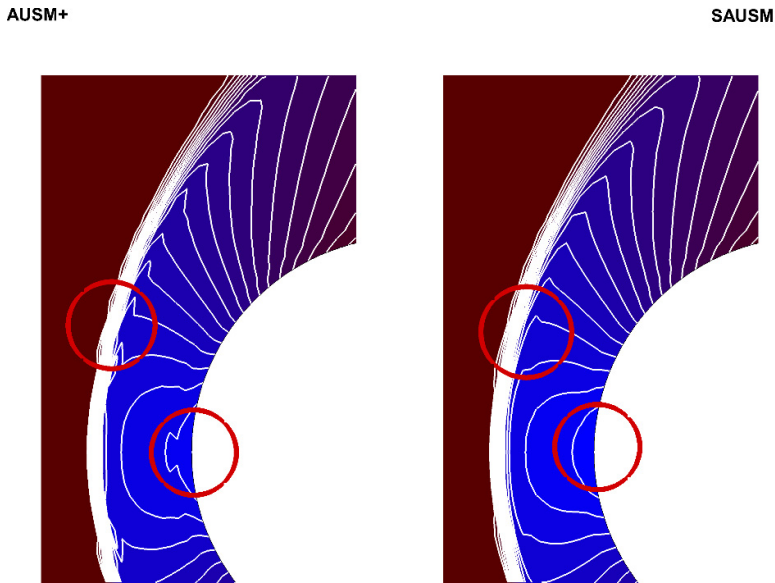


Fig. 9. Comparing the distribution of pressure in hypersonic flow over a cylinder.

of an average speed of sound across cell interfaces introducing excessive numerical dissipation at low Mach numbers, compromising overall accuracy; and inherent inaccuracies in the AUSM+ eigenvalue computations further amplifying the carbuncle instability. In sharp contrast, the SAUSM scheme operates without adjustable parameters. Its enhancements in effectively resolving discontinuities are intrinsically achieved without controlling parameters. This is facilitated by the AUFS component, which inherently adjusts and provides the necessary numerical dissipation based on its internal mechanism. This sets SAUSM apart from other methods,<sup>27,28,37</sup> which rely on tuning empirical constants to manage anomalies like the carbuncle phenomenon. The SAUSM results, on the other hand, exhibit a smooth and continuous bow shock profile without detectable anomalies, bifurcations, or distortions. This showcases the remarkable robustness and stability of SAUSM in effectively capturing shock phenomena, thanks to its unique hybrid formulation. By integrating the AUFS component near shock discontinuities, vital supplemental dissipation is introduced, effectively damping out destabilizing perturbations that trigger anomalies like the carbuncle instability observed with the standalone AUSM+ approach. Despite a pronounced bow shock in this demanding test case, eliminating the carbuncle phenomenon within the SAUSM solution offers unequivocal validation of its capability to accurately and stably simulate intricate compressible flows involving shocks. This accomplishment is made possible through the adaptive dissipation control mechanism inherent to the SAUSM methodology. The comprehensive comparative analysis underscores SAUSM's proficiency in enabling high-fidelity prediction of diverse compressible flow regimes containing discontinuities. Importantly, SAUSM avoids succumbing to the numerical shock anomalies exhibited by AUSM+. This firmly establishes SAUSM's robustness, accuracy and versatility as a potent technique for various computational fluid dynamics applications.

Figure 10 shows the distribution of the weighting function (Eq. 28) along the stagnation streamline for the hypersonic flow over a cylinder test case. Near the shock region on the cylinder surface, the weighting function (Eq. 28) approaches 1, indicating that the flux is heavily weighted towards the AUFS scheme. This provides enhanced shock-capturing stability by leveraging the inherent robustness of AUFS. The artificial wave speeds in AUFS introduce numerical dissipation that effectively damps perturbations that can lead to anomalies like the carbuncle phenomenon. In the smooth upstream region away from discontinuities, the weighting function trends towards  $-1$ , shifting the weighting towards the AUSM+ scheme. With minimal dissipation, AUSM+ maintains accuracy in resolving smooth flow features. The smooth transition between the two schemes and the weighting function provides is vital to achieving stability and accuracy. Near the shock, stability is prioritized, while accuracy is emphasized away from discontinuities. This prevents the emergence of anomalies like the carbuncle instability exhibited in Fig. 9 by the standalone AUSM+ scheme under the high aspect ratio grid. Moreover, Fig. 10 validates that the weighting function in SAUSM appropriately biases the scheme towards AUFS robustness near discontinuities while shifting to AUSM+ accuracy in smooth regions. This seamless

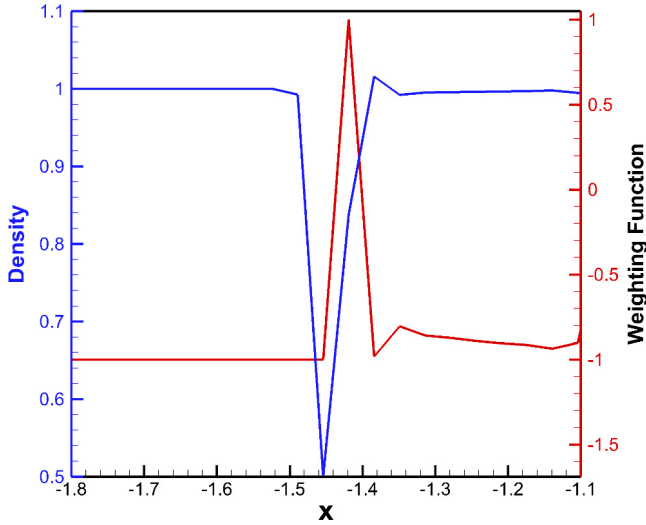


Fig. 10. Distribution of weighting along the stagnation streamline for a Mach 10 hypersonic flow over a circular cylinder problem.

hybridization eliminates anomalies like the carbuncle phenomenon while preserving the resolution of flow features. The adaptive blending is central to the shock-stable and high-fidelity performance of SAUSM demonstrated in the results.

## 5. Conclusion

This study introduced SAUSM, a novel hybrid numerical scheme for accurately and robustly simulating diverse compressible flows governed by the Euler equations. The limitations of existing techniques, including insufficient inherent shock dissipation in low-diffusion methods and inadequate flexibility to adjust robustness in pure flux vector splitting, highlighted the need for an adaptive approach. The proposed SAUSM methodology seamlessly combines the accuracy of AUSM+ in smooth regions with the inherent stability of AUFSS at discontinuities through a continuous weighting function. This provides customized dissipation adjusted to flow conditions. The consistent flux splitting preserves accuracy, while the simple non-matrix structure reduces complexity versus characteristic decompositions. The comprehensive numerical experiments validate SAUSM's capabilities in resolving discontinuities without anomalies across various compressible flow regimes. The 1D Riemann problem verified accurate shock-capturing comparable to the analytical solution. The 2D Riemann problem showcased SAUSM's ability to resolve complex oblique shock interactions without anomalies like the kinked Mach stem that arises in standalone AUSM+ solutions.

The double Mach reflection scenario confirmed stability even in geometrically complex configurations prone to instabilities. Finally, the cylinder test established

resilience against the carbuncle phenomenon through adaptive dissipation control. In summary, SAUSM offers a promising new approach for accurately and robustly simulating compressible Euler flows across various conditions. Its seamless combination of AUSM+ and AUFS schemes provides the best of both worlds, ensuring high-fidelity resolution of flow features while maintaining stability near shocks and discontinuities. The ability to eliminate anomalies like the carbuncle phenomenon while preserving accuracy demonstrates SAUSM's versatility as a general-purpose technique for computational fluid dynamics. Future work should focus on extending SAUSM to handle viscous flows governed by the Navier-Stokes equations. Additional research could explore potential applications of SAUSM in other fluid dynamics and aerospace engineering areas, aiming to further validate its effectiveness in different scenarios. Overall, SAUSM represents a significant advancement in numerical methods for compressible flow simulations, providing a powerful tool for researchers and engineers seeking accurate and stable results in their computational fluid dynamics studies.

## References

1. M.-S. Liou, Open issues in numerical fluxes: Proposed resolutions, in *20th AIAA Computational Fluid Dynamics Conference* (2011), pp. 249–264.
2. F. Qu *et al.*, *Comput. Fluids* **102**, 203 (2014).
3. B. Vanleer, Flux-vector splitting for the 1990s, in *NASA, Lewis Research Center, Computational Fluid Dynamics Symposium on Aeropropulsion* (NASA, 1991).
4. M. Sun and K. Takayama, *J. Comput. Phys.* **189**, 305 (2003).
5. G. Tchien, Y. Burtshell and D. E. Zeitoun, *Int. J. Comput. Fluid Dyn.* **22**, 209 (2008).
6. E. F. Toro, *Riemann Solvers and Numerical Methods for Fluid Dynamics: A Practical Introduction* (Springer Science & Business Media, 2013).
7. R. L. Roe, *J. Comput. Phys.* **43**, 357 (1981).
8. M.-S. Liou and C. J. Steffen, Jr., *J. Comput. Phys.* **107**, 23 (1993).
9. M.-S. Liou, *J. Comput. Phys.* **129**, 364 (1996).
10. K. H. Kim, C. Kim and O.-H. Rho, *J. Comput. Phys.* **174**, 38 (2001).
11. K. Kitamura *et al.*, *AIAA J.* **48**, 763 (2010).
12. K. Peery and S. Imlay, Blunt-body flow simulations, in *24th Joint Propulsion Conference, American Institute of Aeronautics and Astronautics* (1988), pp. 2904–2920.
13. J. J. Quirk, A contribution to the great Riemann solver debate, *International Journal for Numerical Methods in Fluids* (Springer, 1997), pp. 555–574.
14. K. Kitamura, P. Roe and F. Ismail, *AIAA J.* **47**, 44 (2009).
15. M. Pandolfi and D. D'Ambrosio, *J. Comput. Phys.* **166**, 271 (2001).
16. M.-S. Liou, *J. Comput. Phys.* **160**, 623 (2000).
17. M. Dumbser, J.-M. Moschetta and J. Gressier, *J. Comput. Phys.* **197**, 647 (2004).
18. K. Xu, *Gas Evolution Dynamics in Godunov-Type Schemes and Analysis of Numerical Shock Instability* (National Aeronautics and Space Administration, NASA, 1999).
19. M. V. Ramalho, J. H. Azevedo and J. L. Azevedo, Further investigation into the origin of the carbuncle phenomenon in aerodynamic simulations, in *49th AIAA Aerospace Sciences Meeting Including the New Horizons Forum and Aerospace Exposition* (2011), pp. 1184–1216.
20. R. Sanders, E. Morano and M.-C. Druguet, *J. Comput. Phys.* **145**, 511 (1998).

21. Z. Shen, W. Yan and G. Yuan, *J. Comput. Phys.* **309**, 185 (2016).
22. N. Fleischmann *et al.*, *J. Comput. Phys.* **401**, 109004 (2020).
23. W. Xie *et al.*, *Comput. Math. Appl.* **102**, 65 (2021).
24. H. Wu, L. Shen and Z. Shen, *Commun. Comput. Phys.* **8**, 1264 (2010).
25. S. Guo and W.-Q. Tao, *Numer. Heat Transf. Part B Fundam.* **73**, 33 (2018).
26. S. Guo and W.-Q. Tao, *Int. J. Heat Mass Transf.* **166**, 120757 (2021).
27. S. Phongthanapanich, *Int. J. Numer. Methods Fluids* **93**, 978 (2021).
28. S. Phongthanapanich, A. Matthujak and K. Ohtani, *AIAA J.* **61**, 1 (2023).
29. J. R. Edwards and M.-S. Liou, *AIAA J.* **36**, 1610 (1998).
30. M. Javarehshkian and A. Mohammadi, *J. Solid Fluid Mech.* **10**, 303 (2020).
31. M. Balaj and M. H. Djavarehshkian, *Int. J. Numer. Methods Fluids* **93**, 2249 (2021).
32. P. D. Lax and X.-D. Liu, *SIAM J. Sci. Comput.* **19**, 319 (1998).
33. F. Qu *et al.*, *Arch. Comput. Methods Eng.* **29**, 1 (2021).
34. P. Woodward and P. Colella, *J. Comput. Phys.* **54**, 115 (1984).
35. K. Kitamura and E. Shima, *J. Comput. Phys.* **245**, 62 (2013).
36. S. Henderson and J. Menart, Grid study on blunt bodies with the Carbuncle phenomenon, in *39th AIAA Thermophysics Conference* (2007), pp. 3904–3929.
37. S. Phongthanapanich, *Shock Waves* **29**, 755 (2019).